Vanillin-Based Photocurable Anticorrosion Coatings Reinforced with Nanoclays

RESEARCH ARTICLE

Macromolecular Materials and Engineering
Open Access
www.mame-journal.de

Vanillin-Based Photocurable Anticorrosion Coatings Reinforced with Nanoclays

Camilla Noè, Leonardo Iannucci, Samuel Malburet, Alain Graillot, and Sabrina Grassini*

This study investigates the chemical–physical properties and anticorrosion effectiveness of UV-cured coatings produced using epoxidized vanillin (DGEVA) as biobased precursor, then reinforced by the addition of nanoclay. After optimizing the UV-curing parameters of three different formulations by Fourier transform infrared spectroscopy (FTIR), the thermo-mechanical properties of the coatings are assessed by differential scanning calorimetric analysis (DSC), dynamic thermal mechanical analysis (DTMA), and pencil hardness. The coatings are applied on mild steel substrates and then their barrier properties are investigated by electrochemical impedance spectroscopy measurements, immersing the samples in 3.5 wt% NaCl aerated solutions. The results show the good corrosion protective effectiveness of the biobased coatings. The nanoclay addition has a beneficial effect, as it hinders the diffusion of the aggressive ions from the electrolyte solution to the metal substrate. The reported findings demonstrate the possibility of using biobased precursors and UV-curing technology to reduce the environmental impact of the coating industry.

1. Introduction

In the field of organic coatings for corrosion protection, epoxy resins are leading the market thanks to their superior stability in corrosive environments and enhanced mechanical, chemical, and thermal properties. Moreover, they have low shrinkage upon curing and good adhesion to various substrates. Nevertheless, their widespread use is raising an increasing number of concerns, as the majority of epoxy resins currently in the market derive from petroleum-based monomers which are dangerous for human health and for the environment.[1,2] In the circular economy context, using biobased epoxy monomers is a promising alternative to move towards sustainable materials.[3] In this view, different biobased monomers with different molecular structures have been recently investigated as coating, both with aromatic (e.g., vanillin,[4] cardanols,[5] lignin,[6] eugenol,[7] resorcinol[1]) and aliphatic structures (vegetable oils[8–10]). Among aromatic structures, one of the most promising building block is the epoxidized vanillin (DGEVA) monomer, which has already attracted the interest of different researchers since its structure resembles the one of bisphenol A diglycidylether (DGEBA), which is currently the leading resin in the epoxy market.[11–13] As a matter of fact, DGEBA is a non-renewable monomer composed of bisphenol A, which is a very toxic substance for humans. Therefore, finding a valid substitute for DGEBA can be considered a high priority for the coating industry to improve the workers' safety during coating application and to reduce the carbon footprint related to monomer production. The use of DGEVA as a green monomer has already been investigated,[14,15] especially for food-contact[16] and for coatings with antibacterial properties.[4,17] Moreover, vanillin-based building blocks have also been proven as efficient environmental-friendly corrosion inhibitors.[18–21] Thus, the use of this precursor in the field anticorrosion coatings unveils promising new possibilities.

Most of the materials described in literature for anticorrosion applications follow a thermal curing process, which allows to realise thicker coatings if compared to UV-curing, but at the same time is more energy-demanding. Considering the field of biobased anticorrosion coatings, many studies reported the use of cardanol and soybean oil as precursors.[22–25] Moreover, in order to enhance the mechanical properties of the material as well as its barrier capabilities, the addition of small amounts of nanofillers is often taken into account. Graphene oxide (GO) nanoplatelets have attracted a lot of attention in the recent years, thanks to their high surface to volume ratio, however they tend to agglomerate and to form microcurrent corrosion, so their use is still limited.[26–28] A valid alternative to GO is represented by nanoclay, which has a low cost, is nontoxic and possesses high stiffness and hardness. Moreover, nanoclay is characterized by a layered structure, and each nanometric layer has an enhanced surface area with respect to other type of fillers, which boosts its

C. Noè, L. Iannucci, S. Grassini
Politecnico di Torino
Dipartimento di Scienza Applicata e Tecnologia
C.so Duca degli Abruzzi 24, Torino 10129, Italy
E-mail: leonardo.iannucci@polito.it
S. Malburet, A. Graillot
Specific Polymers
150 Avenue des Cocardières, Castries 34160, France

The ORCID identification number(s) for the author(s) of this article can be found under https://doi.org/10.1002/mame.202400155

DOI: 10.1002/mame.202400155

potential as reinforcing agent in polymeric coatings. Moreover, the use of nanoclay as a filler leads to the development of sustainable nanocomposites, an outcome which is consistent with the goal of the coating industry towards a greener production.

Thus, in order to specifically address the coating environmental sustainability, in this work the greenest curing technology was selected: the cationic UV-curing method. In fact, this process is faster, less energy-consuming, and has reduced volatile organic compound (VOC) emissions with respect to the conventional thermal/infrared curing methods. Thus, developing new photocured formulations represents a forward-thinking approach to the coating industry, able to strongly reduce the environmental impact related to coating production.

To the best of Authors' knowledge, the use of UV-curing technology to develop biobased fully DGEVA coatings for corrosion protection has not been explored yet. To fill this gap, in this work, DGEVA-nanoclay composites were developed, using different nanofiller content. After optimizing the curing parameters, the thermal and thermomechanical properties of the coatings were carefully investigated as well as their hardness, contact angle, and corrosion protection effectiveness.

2. Experimental Section

2.1. Materials

Diglycidylether of vanillyl alcohol (DGEVA, SP-9S-5-005) was used as biobased epoxy monomer; it was synthesized following a two-step procedure and provided by SPECIFIC POLYMERS. Triarylsulfonium hexafluoroantimonate salt mixed 50 wt% in propylene carbonate (cationic photoinitiator), surface modified nanoclay (Montmorillonite) containing 35–45 wt% dimethyl dialkyl (C14-C18) amine, vanillyl alcohol (98%) benzyltriethylammonium chloride (TEBAC) (99%), anhydrous sodium sulfate Na_2SO_4 (99%), epichlorohydrin (ECH), sodium hydroxide pellets (NaOH), and all solvents (>95%) used were purchased from Sigma Aldrich and used as received.

2.2. Synthesis of Diglycidylether of Vanillyl Alcohol (DGEVA)

The diglycidylether of vanillyl alcohol was synthesized following a previously reported method.[15,29] Briefly, 10 g of vanillil alcohol was initially mixed with 1.5 g of TEBAC. Then ECH was added and the solution was heated up to 30 °C. After 4 h of magnetic stirring, the solution was cooled down to 15 °C and NaOH (33 wt%) water solution was slowly added. The reaction was left to proceed overnight at 15 °C, then deionized water and ethyl acetate were added. The organic layer was subsequently washed twice with deionized water and dried with sodium sulfate (Na_2SO_4). The solvent was removed by rotary evaporation.

2.3. Coating Preparation

To prepare the coating formulation, DGEVA was first heated at 60 °C to achieve a liquid state, then different concentrations of nanoclay were added (see **Table 1**). To obtain a homogeneous dispersion of the nanoclay in the resin, the formulations were sonicated at 50 °C for 2 h. Then, the triarylsulfonium hexafluoroantimonate salt (Figure S1, Supporting Information), used as the cationic photoinitiator, was added in a concentration of 6 phr (per hundred resin, actual phI content = 3 phr) followed by an additional sonication of 10 min. After that, the formulations were magnetically stirred for 5 min at 60 °C, and then the films were cast onto a mild steel substrate (composition: 0.10 wt% C, 0.60 wt% Mn, 0.20 wt% Ni, 0.15 wt% Cr, and balance Fe). Before applying the coating, the metal substrates were polished with emerit papers up to 800 grit, and then cleaned in acetone. The formulation (consisting of epoxy monomer, photoinitiator, and nanoclay) was applied using a spiral bar coater to ensure a homogeneous thickness of 50 µm. Subsequently, the film was crosslinked under a Dymax ECE 5000 Flood lamp for 1 minute with a light intensity (UVA) of 130 mW cm^{-2}.

Table 1. Composition of the photocurable formulations.

Sample name	Epoxy monomer	Photoinitiator [wt%]	Nanoclay [wt%]
V0	DGEVA	6	0
V1	DGEVA	6	1
V3	DGEVA	6	3

2.4. Characterizations

2.4.1. Proton Nuclear Magnetic Resonance (^{1}H-NMR)

^{1}H-NMR spectrum of the DGEVA monomer was obtained in CDCl3-d6 using Bruker Advance 300 (300 MHz) spectrometer equipped with a QNP probe at room temperature (RT).

2.4.2. Fourier Transform Infrared Spectroscopy (FTIR)

The Fourier transform infrared spectroscopy (FTIR) spectra were recorded using a Nicolet iS 50 Spectrometer instrument operating in transmission mode. The DGEVA formulations were coated on a silicon wafer (average film thickness of 20 µm). The data were collected in the 500–4000 cm^{-1} wavelength range before and after irradiation under the static DYMAX lamp. All measurements were obtained in air with a scanning rate of 1 scan per 1.2 s with a spectral resolution of 4.0 cm^{-1}. The Thermo Scientific OMNIC Specta Software was used to record and process the data. All measurements were recorded in triplicates. The epoxy group conversion was calculated by following the decrease of the 910 cm^{-1} peak. As reference, the peak at 1511 cm^{-1} was selected, as it represents the C=C double bond in the aromatic ring and it is not affected by the reaction. Then the conversion rate was computed as follows (Equation 1)

$$\text{Conversion } (\%) = \left(1 - \frac{\frac{A_{i\_post}}{A_{i\_pre}}}{\frac{A_{0\_post}}{A_{0\_pre}}}\right) \times 100 \quad (1)$$

where A_{i_pre} and A_{i_post} are the area of the epoxy group peak before and after the crosslinking reaction, respectively. A_{0_pre} and A_{0_post} are the area of the reference peak before and after the reaction.

2.4.3. Differential Scanning Calorimetric Analysis (DSC)

Differential scanning calorimetric analysis (DSC) was carried out on a Mettler Toledo DSC instrument at a heating rate of 10 °C min^{-1} using a N_2 atmosphere (50 mL min^{-1}). Samples (weighting 8–10 mg) were inserted in a 100 µL aluminum pan with pierced lids.

2.4.4. Dynamic Thermal Mechanical Analysis (DTMA)

Dynamic thermal-mechanical analysis was performed using a Triton Technology. Samples with dimensions 10 mm × 7 mm × 0.1 mm were tested with uniaxial stretching performed with a heating rate of 3 °C min^{-1}, frequency of 1 Hz and strain of 0.02%. The storage modulus (E') and the loss factor (tanδ) were recorded as a function of temperature. The peak of tanδ can be taken as the glass transition temperature of the material.

2.4.5. X-Ray Diffraction (XRD)

The dispersion of the nanoclay in the crosslinked material was assessed using X-ray diffraction. The analyses were performed after removing the coating from the metal substrate using a blade. The instrument was a Panalytical X'Pert PRO PW 3040/60 X-ray diffractometer operated at 40 kV and 40 mA using a monochromatic Cu-Ka radiation of 1.54 Å. The 2Theta range was from 4.5° to 30°, with a step size of 0.026° and 140 s per step.

2.4.6. Pencil Hardness

The pencil hardness test was performed by using pencils of different grades starting from the 6H and continuing down the scale testing with softer and softer pencils according to ASTM D 3363–74. The pencils were maintained at 45° and pushed for at least 6 mm with uniform pressure and speed onto the coating surface. The hardness of the coating was taken as the one of the hardest pencil which caused a cut less than 3 mm long out of the 6 mm test push on the surface of the coating.

2.4.7. Solvent Rub Resistance Test

The coating chemical resistance was evaluated by methyl-ethyl-ketone double rub test according to the ASTM D5402. Double rubs were performed until the substrate was exposed, or for a maximum of 200.

2.4.8. Contact Angle

Contact angle measurements were performed using a Kruss DSA10 instrument, equipped with a video camera. Analyses were made at room temperature by means of the sessile drop technique. Six measurements were performed on each sample. The surface free energy was determined on the basis of Owens-Wendt-Rabel-Kaelble (WORK) method.[32] The measuring liquids were double distilled water (γ = 72.8 mN m^{-1}) and diiodomethane (γ = 50.8 mN m^{-1}).

2.4.9. Electrochemical Characterizations

Electrochemical measurements were used to assess the corrosion protective effectiveness of the organic coatings applied on a mild steel substrate. All measurements were carried out with an Ivium-n-Stat potentiostat, in a 3-electrode electrochemical cell, using an Ag/AgCl electrode as the reference electrode, a Pt wire as the counter electrode, and the coated steel sample as the working electrode. Tests were performed in a 3.5 wt% NaCl (sodium chloride) aerated solution at room temperature. The exposed sample surface was equal to 0.78 cm^2; all reported data are scaled to the equivalent area of 1 cm^2.

Samples were exposed to the electrolyte for one week and EIS measurements were acquired after 24 and 168 h, in order to monitor the protection effectiveness of the three coatings formulations and their stability in contact with the aggressive environment. EIS measurements were performed in the frequency range from 10^5 to 10^{-2} Hz using a sinusoidal signal with an amplitude of 20 mV, acquiring 10 points per frequency decade.

Impedance spectra were then fitted using an appropriate equivalent electrical circuit (EEC) model. In the EEC, circuit parameters model the electrochemical system composed of the coated metal and the electrolyte and allow to quantitatively assess the protective performance of the coating. EEC fitting was performed using the IviumSoft 4.1038.

2.4.10. Field Emission Scanning Electron Microscope (FESEM)

The field emission scanning electron microscope (FESEM, Supra 40, ZEISS) was used to characterize the surface morphology of the coatings after 168 h of immersion in the NaCl solution. The images were acquired using the InLens detector, setting the acceleration voltage to 5 kV and the aperture size to 30 µm.

3. Results and Discussion

Fully biobased coatings reinforced with nanoclay were obtained with a UV-activated cationic reaction. The epoxy vanillin monomer was synthesized by replacing the hydroxyl group of vanillyl alcohol in a two-step one-pot process already reported previously (**Scheme 1**).

The success of the curing reaction was confirmed by ^{1}H-NMR spectroscopy (see Figure S2 in the Supporting Information). In fact, in the spectrum of DGEVA (M_w = 272.6 g mol^{-1}), the typical epoxy rings protons were clearly visible at δ^1 = 2.64, 2.82, and 3.21 ppm and the R–CH_2–O protons at δ^1 = 4.42 and 3.75 ppm. The epoxy ring content was evaluated by ^{1}H-NMR titration and was equal to 7.28 m_{eq} g^{-1} with an average number of repeating units of 0.03. This synthesis protocol allows to obtain a very

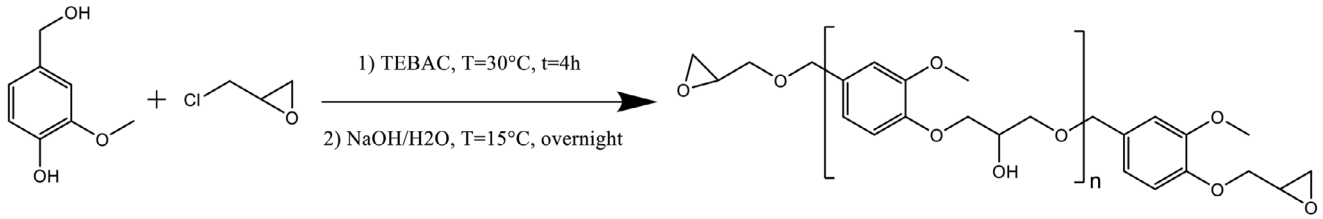

Scheme 1. Reaction scheme of DGEVA. The DGEVA final structure may vary depending on which alcohol the epichlorohydrin reacts with ($n = 0.03$).[29]

high yield (94%) and has promising industrial scalability. Even if this synthesis involves the use of ECH, which might pose a constraint on the overall eco-friendliness of the process, currently, this reagent is indispensable for accomplishing the epoxidation of numerous biobased monomers.[30,31] Future investigations could explore alternatives to the hazardous ECH, seeking more environmentally friendly reagents to enhance the sustainability.

To study the UV-curing reaction of the pristine DGEVA resin, FTIR spectra recorded before and after the photocrosslinking reaction were analyzed and compared.

In the DGEVA spectrum reported in **Figure 1** in black, the typical peak of vanillyl can be clearly identified. The peaks ranging from 1592 to 1453 cm^{-1} represent the C–C stretching vibration of the substitute benzene. The peaks at 1260 and 1230 cm^{-1} can be assigned to the wagging and twisting vibrations of $–CH_2$ group. From 1260 to 1160 cm^{-1} the vanillyl fingerprint region is located. The peak at 1600 cm^{-1} represents the C–O stretching vibration. At higher wavenumber, the small peaks ranging from 3000 and 3060 cm^{-1} can be attributed to the methyl groups close the epoxy rings, while the two high peaks at 2970 and 2930 cm^{-1} can be assigned to the sp^3 C–H vibration of the aliphatic chain.

The success of the photopolymerization reaction was confirmed by the decrease in intensity of the epoxy ring peaks centered at 910 and 850–800 cm^{-1} after the UV-irradiation and by the appearance of a large peak centered at 3470 cm^{-1}, which represents the –OH stretching vibration formed after the opening of the epoxy rings.

The epoxy groups conversion (equal to 54%) was calculated following the decrease of the epoxy group peak in the FTIR spectra as described in the Experimental section. In Figure 1, the spectra of the DGEVA resin before (V0_pre) and after (V0_post) the UV-curing are reported.

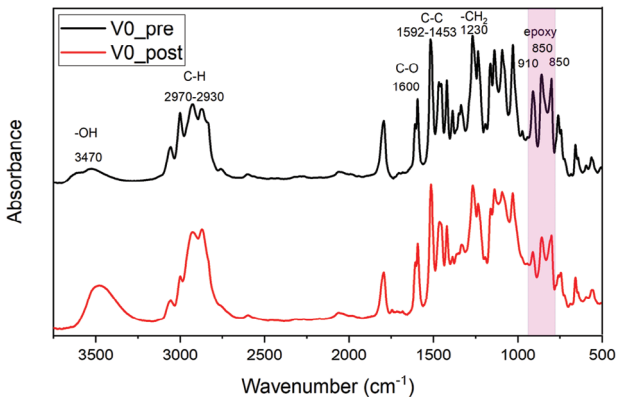

Figure 1. FTIR spectra of the DGEVA film before (V0_pre) and after (V0_post) the photocrosslinking reaction.

It was not possible to estimate the epoxy conversion of the DGEVA composites (i.e., containing the nanoclay as filler), since in this case the fingerprint region of the dimethyl dialkyl (C14-C18) amine, which was covering the surface of the nanoclays, was overlapping with the epoxy peaks.[32] In this work, it was selected a modified nanoclay to avoid the use of dispersant which may compromise the overall performance and durability of the coating and possess adverse environmental impacts.

The possibility to further boost the epoxy group conversion with a thermal treatment was also investigated.

The time and temperature for the post-treatment were optimized using DSC analysis. In fact, in the DSC thermograms of the DGEVA composites films (V1, and V3), it was possible to observe an exothermic peak centered at around 120 °C, suggesting un uncompleted reaction probably caused by an early vitrification of the network (Figure S3, Supporting Information). For this reason, the post-curing treatment was performed for all samples at 120 °C for 7 min. After this time, in the DSC thermogram, it was not possible to see anymore an exothermic peak. After the postcuring the epoxy group conversion of the DGEVA network (V0) increased up to 66% (Figure S4, Supporting Information).

Using DSC analysis it was also possible to investigate the thermal properties of the cured composites films. **Table 2** reports the glass transition temperature (T_g) of all the thermosets. As can be observed, the T_g increases when 1 wt% of nanoclay is added, while the addition of 3 wt% seems not to affect the crosslinked network. This result suggests that in the composites V1 a good dispersion of the nanoclay is obtained, and the filler successfully hinders the polymer chain mobility, enhancing its T_g. On the other hand, in the V3 composites, a certain amount of nanoclay aggregates (see XRD analyses reported below), leading to network inhomogeneities and thus limiting the reinforcement effect induced by the nanoclay addition.

Table 2. Thermal and mechanical properties of the crosslinked DGEVA composite films.

Formulation	T_{g_DSC} [°C]	T_{g_DTMA} [°C]	$E'_{glassy\_plateau}$ [MPa]	$E'_{rubery\_plateau}$ [MPa]
V0	104 ± 1.0	69 ± 2.1	293 ± 7	0.2 ± 0.01
V1	110 ± 0.7	81 ± 1.4	518 ± 4	1.4 ± 0.2
V3	103 ± 1.2	69 ± 3.2	484 ± 6	1.2 ± 0.1

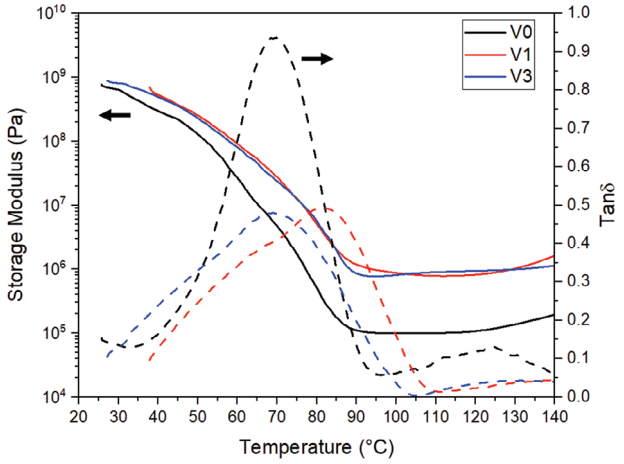

Figure 2. E' and Tanδ of the DGEVA composite coatings. For each sample, the solid line represents E', while the dashed line represents Tanδ.

The thermo-mechanical properties of the films were investigated through DTMA analysis, which allows to evaluate the elastic and viscous components, namely storage E' and loss E'' modulus of the materials, respectively. The ratio between E''/E' is called the damping factor (Tanδ) and its maximum is used to estimate the T_g of the material (data reported in **Table 2**). The DTMA graphs showing the Tanδ and the E' modulus of the coatings are reported in **Figure 2**. As can be observed, the Tanδ maximum shifts towards higher temperature with the addition of 1 wt% of nanoclay, and remains almost unaffected by the addition of 3 wt% of it. This is in good agreement with the DSC results. Moreover, it is possible to observe a decrease of the Tanδ height with the addition of the filler, which can be attributed to a network homogeneity reduction. Furthermore, the E' values of the V1 and V3 formulations are higher than the V0 (see **Table 2**), which can also be ascribed to a reinforcement effect of the nanoclay towards the biobased resin. Indeed, this E' enhancement indicates that the polymer chain movements are hindered by the filler-matrix interaction suggesting a good stress transfer between the filler and the matrix. Furthermore, also the fact that the E' value of V1 is almost identical to the V3 one, may also indicate the formation of nanoclay aggregates in the V3 formulation.[33]

To further investigate the morphology of the epoxy-nanoclay composite, XRD analyses were performed. Actually, using this technique it is possible to assess the dispersion of the filler in the polymeric matrix, discriminating between an exfoliated or intercalated morphology.[34] As can be seen from **Figure 3**, all coatings are characterized by a broad peak centered at about 20°, related to the amorphous epoxy network. Instead, at lower angles, a signal related to the diffraction of lamellar planes (the (001) plane in montmorillonite) is present only for the V3 samples (2Theta = 5.7°). The absence of this peak in V1 samples suggests the presence of an exfoliated morphology in these coatings (V0 samples do not contain nanoclay, and present a similar diffractogram). Moreover, looking at the XRD pattern acquired on pure nanoclay samples, it is possible to identify the characteristic peaks of montmorillonite: at 19.7° and at 7.1°, attributed to the (100) and (001) reflection plane respectively.[35] As in the V3 samples the latter peak is shifted towards lower diffraction angles, this is additional evidence of the intercalation of clay lamellae by the polymer chains, which leads to an increased interlamellar distance.[36,37]

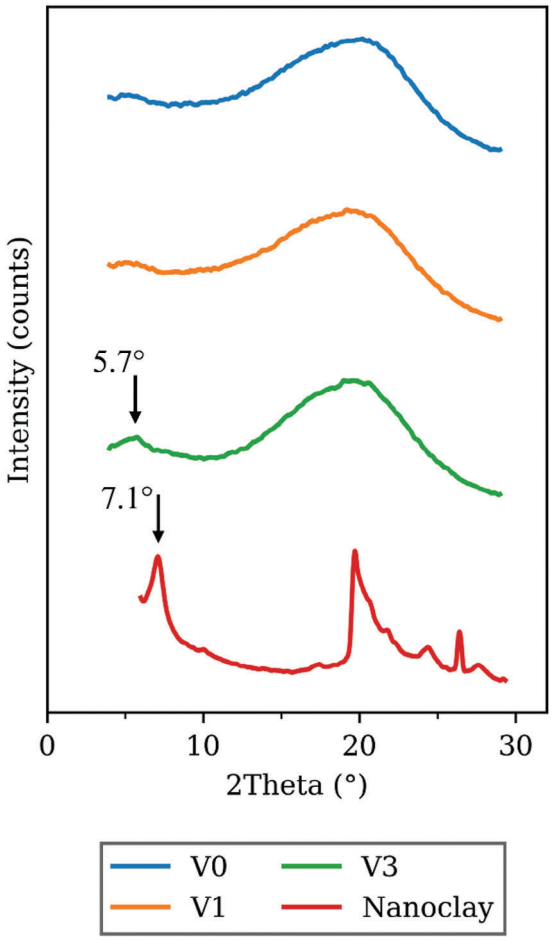

Figure 3. XRD diffractograms acquired on V0, V1, V3 samples and on the nanoclay.

Considering the physical-chemical characterizations (see **Table 3**), all the UV-cured coatings showed excellent solvent resistance, all above 200 rub, and good surface hardness. Previous articles reported a decrease in hardness values with

Table 3. Properties of the DGEVA crosslinked composites coatings.

Formulation	Solvent resistance	Hardness	Contact angle$_{water}$ [°]	Contact angle$_{diiodomethane}$ [°]	Surface tension [mN m^{-1}]
V0	>200	6H	71.7 ± 1.5	55.5 ± 3.9	40.5
V1	>200	6H	72.6 ± 2.7	53.3 ± 3.2	40.9
V3	>200	6H	71.5 ± 2.4	53.5 ± 2.6	41.3

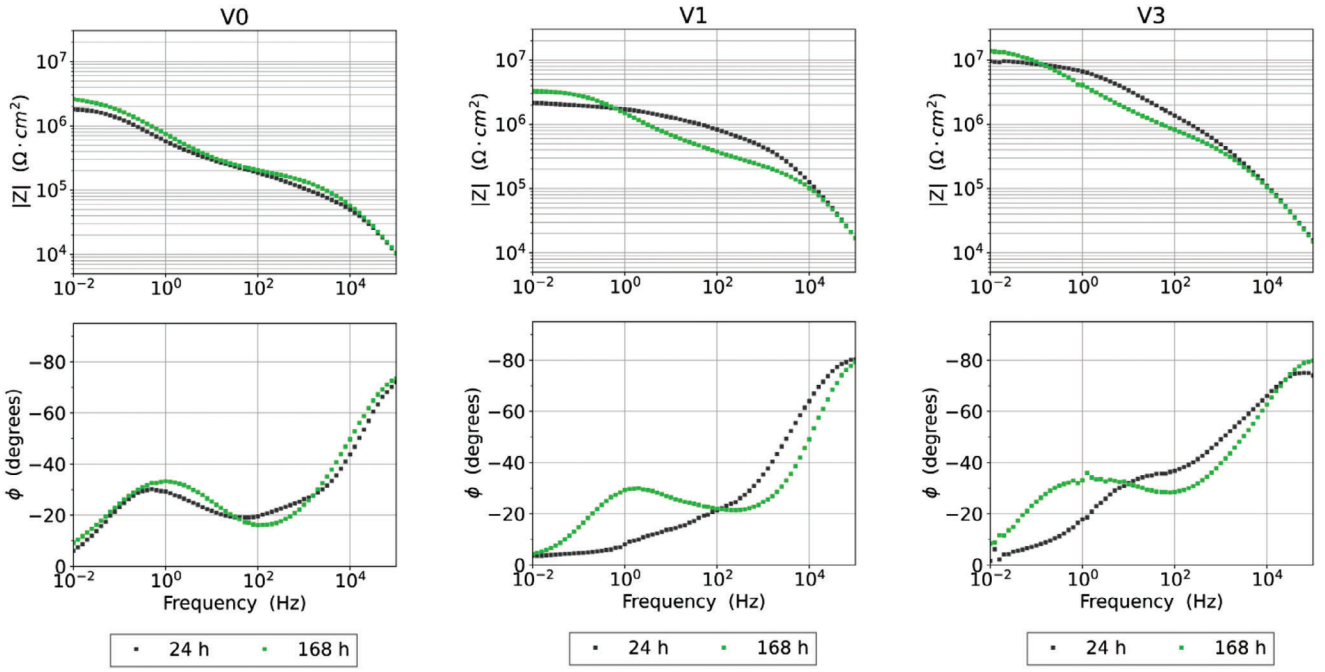

Figure 4. Impedance spectra (represented as Bode diagrams) acquired on the 3 coatings (V0, V1, and V3) after 24 h and after 168 h of immersion in the 3.5 wt% NaCl solution.

increased nanoclay content due to a decrease in the degree of crosslinking inducing a softening effect.[33] However, in this case, no hardness reduction was recorded from DGEVA coating reinforced with nanoclay; this results may indicate a good reinforcement effect of nanoclay compensating the reduced crosslinking.

The water contact angle achieved for all coatings are in the same order of magnitude as other UV-cured fossil-fuel based resin like 3,4-epoxycyclohexylmethyl-3,4-epoxycyclohexane carboxylate.[38] To calculate the surface tension (γ) of the biobased reinforced composites, the diiodomethane contact angle was also investigated. The obtained γ values are all around 40 nm m^{-1} which are consistent with the one previously reported in other biobased coatings for corrosion protection.[39]

3.1. Anticorrosion Properties

The corrosion protective effectiveness of the 3 coatings was assessed by means of EIS. Actually, using this electrochemical technique it is possible to monitor noninvasively the stability of the coating and the corrosion kinetics on the metal substrate when the material is in contact with an aggressive solution. A high impedance modulus in the low-frequency range is characteristic of coatings which are able to effectively protect the substrate and hinder the corrosion processes.[40] The impedance spectra acquired on the 3 coatings at the beginning and at the end of the corrosion tests are reported in **Figure 4** as Bode diagrams.

As can be seen, all coatings exhibit a capacitive-like behaviour at high frequencies (phase values close to −90°), while they shift to a resistive-like behaviour at low frequencies, where the impedance phase reaches values close to 0°. At the beginning of the test (spectra acquired after 24 h of immersion), the impedance modulus at 0.01 Hz ranges between 2×10^6 Ohm cm^2 (for the V0 coating) to 10^7 Ohm cm^2 (for the V3 coating). So, considering these values,[41] all coatings are able to effectively protect the metal substrate in the aggressive electrolyte and the beneficial effect of the filler is evident as well, as the modulus significantly increases with its addition. After 168 h of immersion in the NaCl solution, the impedance modulus remains almost unaltered. Conversely, the main changes can be observed in the trend of the phase, where a second peak becomes evident in the low-frequency range of the spectrum (centred at about 1 Hz). This new feature should be attributed to the faradaic reactions occurring on the surface of the metal after that water and chloride ions are able to diffuse from the solution through the coating.[41,42] It is worth to notice that for the V0 samples, this second peak in the phase trend was present already in the spectrum acquired after 24 h, confirming that in this case the barrier properties against diffusion are weaker due to the absence of filler.

In order to derive a quantitative model which describes the coating and the transport phenomena occurring during the test, EEC fitting was performed. The employed electrical circuit is the one reported in **Figure 5**, which is composed of: R_s representing the electrolyte resistance, R_{coat} and CPE_{coat} modelling the coating resistance and capacitance respectively, and R_{ct} and CPE_{dl} modelling the charge transfer resistance and the double layer capacitance at the interface between the coating and the metal. In the circuit, all capacitors were modelled as a constant phase elements (CPE); its impedance is defined as follows

$$Z_{CPE} = \frac{1}{(j\omega)^n Q} \quad (2)$$

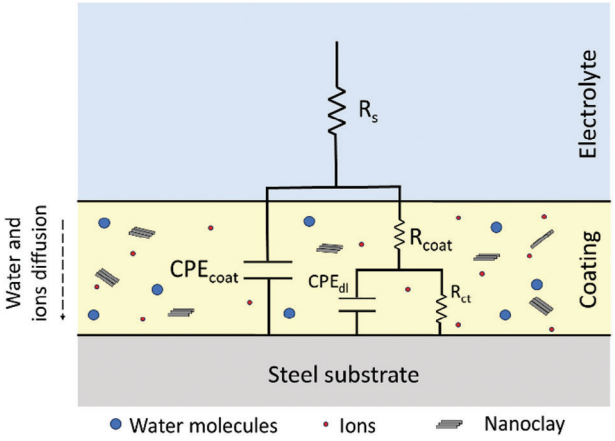

Figure 5. Equivalent electrical circuit model representing the electrochemical system composed of the steel substrate, the coating, and the electrolyte.

where Q is the CPE parameter having dimensions of a capacitance, $j = \sqrt{-1}$, $\omega = 2\pi f$ (f is the frequency) and n is a parameter that ranges between 0 and 1.[43] The use of CPE allows to take into account possible heterogeneity in the coating, surface roughness and time constant dispersion so it is generally used to improve the goodness of fitting for experimental data.[44] The computed values for the circuit parameters are listed in Table S1 in the Supporting Information.

In the developed simulation, R_{coat} and CPE_{coat} model the high-frequency part of the spectrum, while R_{ct} and CPE_{dl} take into account the low-frequency range. As far as R_{coat} is concerned, which is generally used as the main parameter to assess the barrier properties, in **Figure 6** it is possible to see that it increases thanks to the filler addition (from 7.30×10^4 Ohm cm^2 for V0 samples to 5.53×10^5 Ohm cm^2 for V3 samples). Actually,

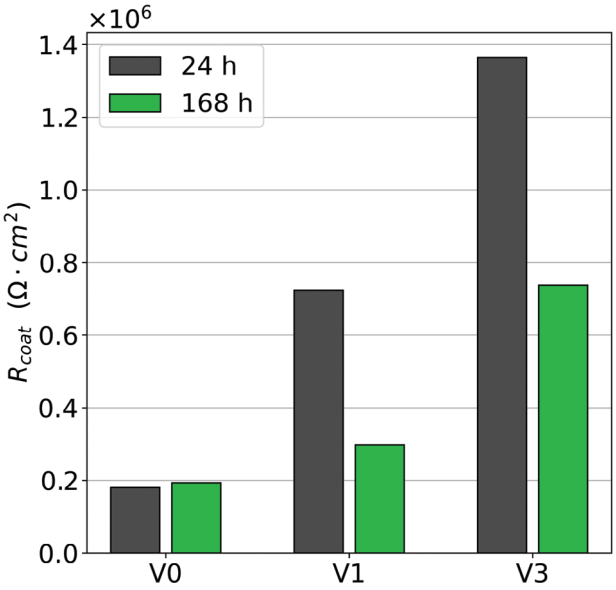

Figure 6. Value of the parameter R_{coat} at the beginning (24 h) and at the end (168 h) of the corrosion tests for the 3 formulations.

the clay nanoparticles increase the tortuosity of the diffusion path across the coating and thus decrease the ionic conductivity in the polymer.[45] After 168 h in contact with the aggressive electrolyte, both V1 and V3 samples exhibit a decrease in the coating resistance (R_{coat}). V0 samples remain stable, as their R_{coat} value was relatively low since the beginning of the test. The rational of this phenomenon is that, after that water and ions diffuse inside the coating, its ionic conductivity increases and thus the coating resistance drops. The water absorption in V0 samples is further highlighted by the higher CPE_{coat} values,[46] which are one order of magnitude higher than the values computed for V1 and V3 samples (see Table S1 in the Supporting Information).

Finally, looking at the R_{ct} parameter, which models the faradic processes on the metal surface, it is possible to see that the highest values (and thus the slowest kinetics for the corrosion reactions) are attributed to the V3 samples, confirming their good barrier properties and protection effectiveness.

The degradation mechanism of the coatings was further assessed by analyzing the samples morphology at the end of the corrosion tests. Two images acquired on V1 and V3 samples by electron microscopy are shown in **Figure 7**

It is possible to see that at the end of the corrosion tests, the coating surface is characterized by the presence of pinholes, i.e., local defects (with dimension in the order of microns) where the saline solution is able to penetrate and thus induce corrosion on the metal substrate. This kind of defect is generally associated to the presence of porosity, which facilitates the formation of a conductive path (created by the aggressive ions) from the solution to the metal surface.[47,48] The formation of these defects was also detected by electrochemical measurements as the second time constant appearing in the low-frequency region of the impedance spectrum, as discussed previously. From electron microscope observation, it was confirmed that the frequency of pinholes was higher in V1 samples, justifying the lower impedance modulus with respect to V3 samples.

Considering these additional observations, in order to further improve the stability of the coatings in aggressive environments, the increase of the nanoclay content could be taken into consideration, as it would increase the tortuosity of the conductive path and thus the time needed to develop it. At the same, a higher filler content would be surely detrimental for the conversion rate of the material; moreover, as shown by XRD analyses, V3 samples exhibit an intercalated morphology (and not exfoliated, as for V1), so a higher nanoclay content would lead to additional aggregation phenomena. For all these reasons, the optimal nanoclay content found in this study is of 3 wt%.

Finally, it is worth to notice that the electrolyte used in the corrosion tests was a very aggressive one, which simulates seawater. For this reason, the measured impedance moduli and thus the protective effectiveness should be considered satisfactory, as the barrier properties in a less aggressive environment would be even better. Moreover, despite the presence of pinholes at microscopic scale, all coatings showed good stability in their electrochemical behavior for the complete duration of the test.

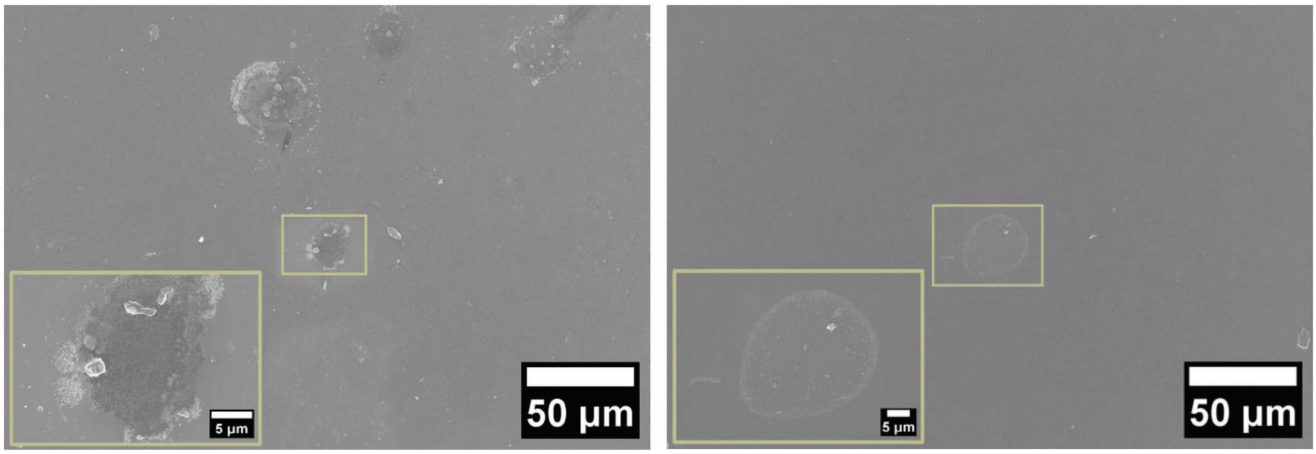

Figure 7. FESEM images acquired on V1 and V3 samples (on the left and on the right, respectively) after the 168 h of immersion in the 3.5 wt% NaCl solution. The inset in the yellow frame shows a micrograph taken at higher magnification.

4. Conclusions

The paper presented a feasibility study to use UV-curing technology for obtaining biobased nanoclay-reinforced composites to produce anticorrosion coatings.

A comprehensive characterization of the mechanical and thermal properties of the coatings derived from vanillin is presented, and it clearly showed the suitability of the material for applications in the coating industry. Furthermore, the hardness and surface tension values achieved by the biobased coatings proved to be comparable with the ones obtained using petroleum-based monomers.

From an electrochemical point of view, the coatings exhibited good protective behavior in a very aggressive environment containing chlorides. The beneficial effect of nanoclay addition was highlighted by EIS measurements and, despite the presence of some pinholes at the end of the corrosion tests, all coatings preserved a stable behavior.

This study provides clear evidence that the use of photocurable biobased composites in the field of corrosion protection coatings is indeed possible and potentially competitive in the market.

Future work will investigate the use of different nanofillers, to delve into reinforcement mechanism and thus further improve the mechanical and barrier properties of these biobased coatings.

Supporting Information

Supporting Information is available from the Wiley Online Library or from the author.

Acknowledgements

The Authors would like to gratefully thank Valeria Gozzano for performing part of the experimental work during her Masters' Degree thesis and Marco Sangermano for the use of some instruments.

Conflict of Interest

The authors declare that they have no known competing financial interests or personal relationships that could have appeared to influence the work reported in this paper.

Author Contributions

C.N. and L.I.: Conceptualization, Investigation, Supervision, Methodology, Writing – original draft. S.M., A.G. : Epoxidation of vanillin; S.G.: Validation.

Data Availability Statement

The data that support the findings of this study are available from the corresponding author upon reasonable request.

Keywords

anticorrosion coatings, biobased coatings impedance spectroscopy, nanoclay, vanillin

Received: April 24, 2024
Revised: June 12, 2024
Published online:

[1] Q.-B. Nguyen, N.-H. Nguyen, A. R. de Anda, V.-H. Nguyen, D.-L. Versace, V. Langlois, S. Naili, E. Renard, *J. Appl. Polym. Sci.* **2020**, *137*, 49051.
[2] R. Auvergne, S. Caillol, G. David, B. Boutevin, J.-P. Pascault, *Chem. Rev.* **2014**, *114*, 1082.
[3] S. Kumar, S. K. Samal, S. Mohanty, S. K. Nayak, *Polym.-Plast. Technol. Eng.* **2018**, *57*, 133.
[4] G. Petrusonyte, A. Kutová, S. Grauzeliene, J. Ostrauskaite, *Polym. Bull.* **2023**, *80*, 12301.
[5] C. Noè, S. Malburet, E. Milani, A. Bouvet-Marchand, A. Graillot, M. Sangermano, *Polym. Int.* **2020**, *69*, 668.
[6] S. Laurichesse, L. Avérous, *Prog. Polym. Sci.* **2014**, *39*, 1266.
[7] J. Qin, H. Liu, P. Zhang, M. Wolcott, J. Zhang, *Polym. Int.* **2014**, *63*, 760.
[8] S. K. Bobade, N. R. Paluvai, S. Mohanty, S. K. Nayak, *Polym.-Plast. Technol. Eng.* **2016**, *55*, 1863.
[9] S. Ma, T. Li, X. Liu, J. Zhu, *Polym. Int.* **2016**, *65*, 164.
[10] S. Malburet, C. Di Mauro, C. Noè, A. Mija, M. Sangermano, A. Graillot, *RSC Adv.* **2020**, *10*, 41954.
[11] E. D. Hernandez, A. W. Bassett, J. M. Sadler, J. J. La Scala, J. F. Stanzione, *ACS Sustainable Chem. Eng.* **2016**, *4*, 4328.

[12] R. Dinu, U. Lafont, O. Damiano, A. Mija, *ACS Appl. Polym. Mater.* **2022**, *4*, 3636.
[13] L. Li, Y. Zhang, Y. Shi, F. Guo, X. Yang, W. Shi, *Mater. Today Commun.* **2023**, *35*, 105692.
[14] C. Noè, M. Hakkarainen, M. Sangermano, *Polymers (Basel)* **2021**, *13*, 1.
[15] C. Noè, S. Malburet, A. Bouvet-Marchand, A. Graillot, C. Loubat, M. Sangermano, *Prog. Org. Coatings* **2019**, *133*, 131.
[16] F. Ng, L. Bonnet, G. David, S. Caillol, *Prog. Org. Coatings* **2017**, *109*, 1.
[17] G. Motiekaityte, A. Navaruckiene, V. Raudoniene, D. Bridziuviene, J. Jaras, K. Kantminiene, J. Ostrauskaite, *J. Appl. Polym. Sci.* **2023**, 140.
[18] S. M. Tawfik, N. A. Negm, *Res. Chem. Intermed.* **2016**, *42*, 3579.
[19] K. Jayanthi, M. Sivaraju, *Rasayan J. Chem.* **2023**, *16*, 892.
[20] S. John, Z. P. Mathew, C. Augustine, J. B. George, B. Joseph, M. K. S. Josh, *Int. J. Biol. Macromol.* **2024**, *262*, 130024.
[21] R. Rosliza, A. Nora'aini, W. B. Wan Nik, *J. Appl. Electrochem.* **2010**, *40*, 833.
[22] J. Lv, Z. Liu, J. Zhang, J. Huo, Y. Yu, *Polymer (Guildf)* **2017**, *121*, 286.
[23] L. R. R. Da Silva, F. Avelino, O. B. F. Diogenes, V. D. O. F. Sales, K. T. Da Silva, W. S. Araujo, S. E. Mazzetto, D. Lomonaco, *Prog. Org. Coatings* **2020**, *139*, 105449.
[24] D. M. Patil, G. A. Phalak, S. T. Mhaske, *J. Coatings Technol. Res.* **2017**, *14*, 517.
[25] J. H. Lingner Moura, M. Heinen, R. C. Da Silva, E. M. A. Martini, C. L. Petzhold, *Prog. Org. Coatings* **2018**, *125*, 372.
[26] W. J. Li, M. M. Aung, M. Rayung, L. H. Ngee, M. L. W. Fui, *Prog. Org. Coatings* **2023**, *175*, 107349.
[27] S. Yang, H. Fang, B.o Shu, Z. Liu, M. Zhou, X. Chen, Y. Hu, Z. Yang, *Prog. Org. Coatings* **2023**, *180*, 107564.
[28] C.-A. Xu, Z. Chu, X. Li, H. Fang, W. Zhou, Y. Hu, X. Chen, Z. Yang, *Prog. Org. Coatings* **2023**, *183*, 107804.
[29] A. Genua, S. Montes, I. Azcune, A. Rekondo, S. Malburet, B. Daydé-Cazals, A. Graillot, *Polymers (Basel)* **2020**, *12*, 2645.
[30] N. Eid, B. Ameduri, B. Boutevin, A. C. S. Sustain, *Chem. Eng.* **2021**, *9*, 8018.
[31] L. Pezzana, G. Melilli, N. Guigo, N. Sbirrazzuoli, M. Sangermano, A. C. S. Sustain, *Chem. Eng.* **2021**, *9*, 17403.
[32] N. Narayanan, S. Gupta, V. T. Gajbhiye, K. M. Manjaiah, *Chemosphere* **2017**, *173*, 502.
[33] A. Rigail-Cedeño, D. F. Schmidt, *AIP Conf. Proc.* **2017**, *1914*, 030023.
[34] J. L. Varela Caselis, E. Rubio Rosas, J. D. Santamaría Juárez, J. A. Galicia Aguilar, M. Sánchez Cantú, O. Olivares Xometl, M. Morales Sánchez, *Corros. Eng., Sci. Technol.* **2018**, *53*, 362.
[35] K. Peng, H. Wang, X. Li, J. Wang, Z. Cai, L. Su, X. Fan, *Sci. Rep.* **2019**, *9*, 16325.
[36] H. Wu, H. Xie, G. He, Y. Guan, Y. Zhang, *Appl. Clay Sci.* **2016**, *119*, 161.
[37] R. Kotsilkova, *J. Appl. Polym. Sci.* **2005**, *97*, 2499.
[38] M. Sangermano, A. Perrot, A. Gigot, P. Rivolo, F. Pirri, M. Messori, *Macromol. Mater. Eng.* **2016**, *301*, 93.
[39] C. Noè, L. Iannucci, S. Malburet, A. Graillot, M. Sangermano, S. Grassini, *Macromol. Mater. Eng.* **2021**, *2100029*, 2100029.
[40] D. Loveday, P. Peterson, B. Rodgers, *CoatingsTech* **2004**, *1*, 46.
[41] E. Akbarinezhad, H. R. Faridi, *Surf. Eng.* **2008**, *24*, 280.
[42] M. Dornbusch, S. Kirsch, C. Henzel, C. Deschamps, S. Overmeyer, K. Cox, M. Wiedow, U. Tromsdorf, M. Dargatz, U. Meisenburg, *Prog. Org. Coatings* **2015**, *89*, 332.
[43] M. E. Orazem, B. Tribollet, *Electrochemical Impedance Spectroscopy*, John Wiley & Sons, New Jersey **2017**.
[44] A. Miszczyk, K. Darowicki, *Prog. Org. Coatings* **2018**, *124*, 296.
[45] R. K. Bharadwaj, *Macromolecules* **2001**, *34*, 9189.
[46] S. Shreepathi, S. M. Naik, M. R. Vattipalli, *J. Coatings Technol. Res.* **2012**, *9*, 411.
[47] S. H. Ahn, J. H. Lee, J. G. Kim, J. G. Han, *Surf. Coatings Technol.* **2004**, *177–178*, 638.
[48] S. R. Taylor, M. W. Wittmann, *Mater. Res. Soc. Symp. Proc.* **1996**, *411*, 31.

